

Frequency- and Amplitude-Dependent Transmission of Stress Waves in Curved One-Dimensional Granular Crystals Composed of Diatomic Particles

Jinkyu Yang · Chiara Daraio

Received: 19 January 2012 / Accepted: 25 June 2012 / Published online: 31 July 2012
© Society for Experimental Mechanics 2012

Abstract We study the stress wave propagation in curved chains of particles (granular crystals) confined by bent elastic guides. We report the frequency- and amplitude-dependent filtering of transmitted waves in relation to various impact conditions and geometrical configurations. The granular crystals studied consist of alternating cylindrical and spherical particles pre-compressed with variable static loads. First, we excite the granular crystals with small-amplitude, broadband perturbations using a piezoelectric actuator to generate oscillatory elastic waves. We find that the linear frequency spectrum of the transmitted waves creates pass- and stop-bands in agreement with the theoretical dispersion relation, demonstrating the frequency-dependent filtering of input excitations through the diatomic granular crystals. Next, we excite high-amplitude nonlinear pulses in the crystals using striker impacts. Experimental tests verify the formation and propagation of highly nonlinear solitary waves that exhibit amplitude-dependent attenuation. We show that the wave propagation can be easily tuned by manipulating the pre-compression imposed to the chain or by varying the initial curvature of the granular chains. We use a combined discrete element (DE) and finite element (FE) numerical model to simulate the propagation of both dispersive linear waves and compactly-supported highly nonlinear waves. We find that the tunable, frequency- and amplitude-dependent filtering of the incoming signals results from the close interplay between the granular particles and the soft elastic media. The findings in

this study suggest that hybrid structures composed of granular particles and linear elastic media can be employed as new passive acoustic filtering materials that selectively transmit or mitigate excitations in a desired range of frequencies and amplitudes.

Keywords Granular crystals · Phononic crystals · Diatomic chains · Highly nonlinear solitary waves · Impact mitigation · Acoustic filtering

PACS numbers · 43.58.Kr · 45.70.-n · 46.40.Cd · 43.20.Ks

Introduction

Granular particles in contacts, arranged in ordered lattices (i.e., granular crystals), are efficient media for the transmission of nonlinear stress waves [1, 2]. One-dimensional (1D) chains of elastic spheres under zero or weak static compression have been shown to support the formation and propagation of compact nonlinear waves in the form of solitary waves [1–6]. These solitary waves derive from the nonlinear (Hertzian) contact interaction between particles (i.e., $F \propto \delta^{3/2}$, where F is the compressive force and δ is the approach between the particles) and a zero tensile response [1, 2]. Such formation of stable nonlinear waves in ordered 1D systems is in contrast to the highly dispersive and dissipative stress propagation observed in disordered granular media [7].

Highly nonlinear solitary waves in granular crystals exhibit unique physical properties compared to the conventional stress waves in linear elastic media. First, solitary waves have constant spatial wavelength, confined to approximately five particle diameters [2, 8]. Second, solitary waves have extremely slow propagation speed, typically an order of magnitude slower than that of dilatational waves within particles [2, 6]. Furthermore, the propagation speed of solitary waves is amplitude-dependent. For a homogeneous granular chain, the

J. Yang · C. Daraio (✉)
Engineering and Applied Science,
California Institute of Technology,
1200 E. California Blvd.,
Pasadena, CA 91125, USA
e-mail: daraio@caltech.edu

J. Yang
Mechanical Engineering, University of South Carolina,
300 Main Street, A224,
Columbia, SC 29208, USA



wave speed can be expressed as $V_s \propto F_m^{1/6}$ (V_s and F_m are the speed of solitary waves and their maximum force amplitude, respectively) [2]. Lastly, solitary waves have unique interaction properties, allowing the formation of single solitary pulses, trains, and shock-like signals [8–13]. By leveraging these characteristics, granular crystals have been proposed for several engineering applications, such as nonlinear lenses for acoustic imaging [14, 15], impact mitigation devices [16–20], and actuators and sensors for nondestructive evaluations [21–23].

Previous studies have shown that granular crystals can also propagate linear elastic waves when they are excited by small-magnitude dynamic forces, relative to the static pre-compression applied to the system [2, 24, 25]. In this case, diatomic granular crystals (i.e., periodic chains with two particles per unit cell) support the formation of a frequency band structure with allowable and forbidden frequency bands of signal propagation (i.e., pass- and stop-bands) [24]. Since stress waves in forbidden frequency bands are prohibited to transmit, such granular crystals can function as passive acoustic filter structures. The selection of material properties, geometry, and boundary conditions of the granular crystals allows controlling the number and location of frequency pass-/stop-bands. Herbold et al. investigated the tunable frequency band-gaps in diatomic granular crystals in various combinations of dynamic and static forces applied to the chain [24]. Boehler et al. controlled the frequency band structures of a granular crystal composed of three-particle unit cells by simply manipulating the particle geometry and pre-compression [25].

This study investigates the comprehensive mechanism of wave formation and transmission in a diatomic granular crystal under various geometrical configurations and impact conditions, encompassing linear to highly nonlinear dynamical regimes. While previous studies focused mainly on a straight, 1D chain of particles, here we consider a curved granular system guided by soft elastic media to account for the coupling mechanism between the granular particles and their surrounding elastic media. By using such a hybrid structure, we demonstrate experimentally the amplitude- and frequency-dependent filtering of compressive waves. First, we report the formation of acoustic band structures in the coupled granular and elastic media in the linear regime. We show that the acoustic band structure can be tuned *in situ* by manipulating the applied static pre-compression or the initial curvature imposed on the elastic guides. Then, we increase the amplitude of the excited dynamic disturbances relative to the static pre-compression. As the dynamic amplitude increases, we observe the disappearance of the linear acoustic band structure and the generation and propagation of highly nonlinear solitary waves. We show experimentally that the suppression of frequency band

structures is critically dependent on the level of nonlinearity in the system, represented by the ratio of dynamic force magnitudes to the static pre-compression. We also demonstrate that the transmission efficiency of solitary waves can be controlled by the curvature initially imposed to the diatomic granular system. The frequency- and amplitude-dependent behavior of the granular system is verified by numerical simulations. We use a numerical model that integrates discrete element (DE) and finite element (FE) methods to simulate the propagation of both dispersive linear waves and compactly-supported highly nonlinear waves [26]. The experimental and numerical results in this study demonstrate that the studied systems can be excellent candidates for creating a new class of engineered materials, which can transmit selected ranges of amplitudes and frequencies from external excitations.

The rest of the manuscript is structured as follows: We describe the experimental setup in Section II. We discuss the formation of frequency band structures and the propagation of highly nonlinear solitary waves in Section III. In Section III, we also describe the numerical approach based on a combined DE and FE model. Section IV compares analytical, numerical, and experimental results, focusing on the effect of pre-compression, chain curvature, and striker masses on the propagation of stress waves through the granular system. Lastly, in Section V, we conclude the manuscript with a summary.

Experimental Setup

The overall configuration of the experimental setup is shown in Fig. 1. The test setup consists of two parts: a granular crystal composed of diatomic unit cells and an apparatus for applying external excitations to the top particle of the granular crystal. The granular crystal consists of an array of alternating spheres and cylinders made from stainless steel (type 440 C, McMaster-Carr). The spherical elements have a radius $R_s=9.53$ mm, mass $m_s=28.2$ g, elastic modulus $E_s=200$ GPa, and Poisson's ratio $\nu_s=0.28$. The cylindrical elements have a radius $R_c=9.53$ mm, a height $h_c=19.1$ mm, and mass $m_c=42.4$ g, with material properties identical to those of the spherical elements. The granular crystal tested is 21 particles long with 10 repeating unit cells ($N=10$) and one additional spherical particle ($i=21$) positioned at the bottom of the chain (see Fig. 1).

In this study, we consider two different configurations of the granular crystal: a straight chain (Figs. 1(a)) and a curved chain (Figs. 1(b)), to investigate the effect of chain curvature on stress transmission. The straight chain serves as a reference system by restricting the lateral motions of granular particles using rigid guides made

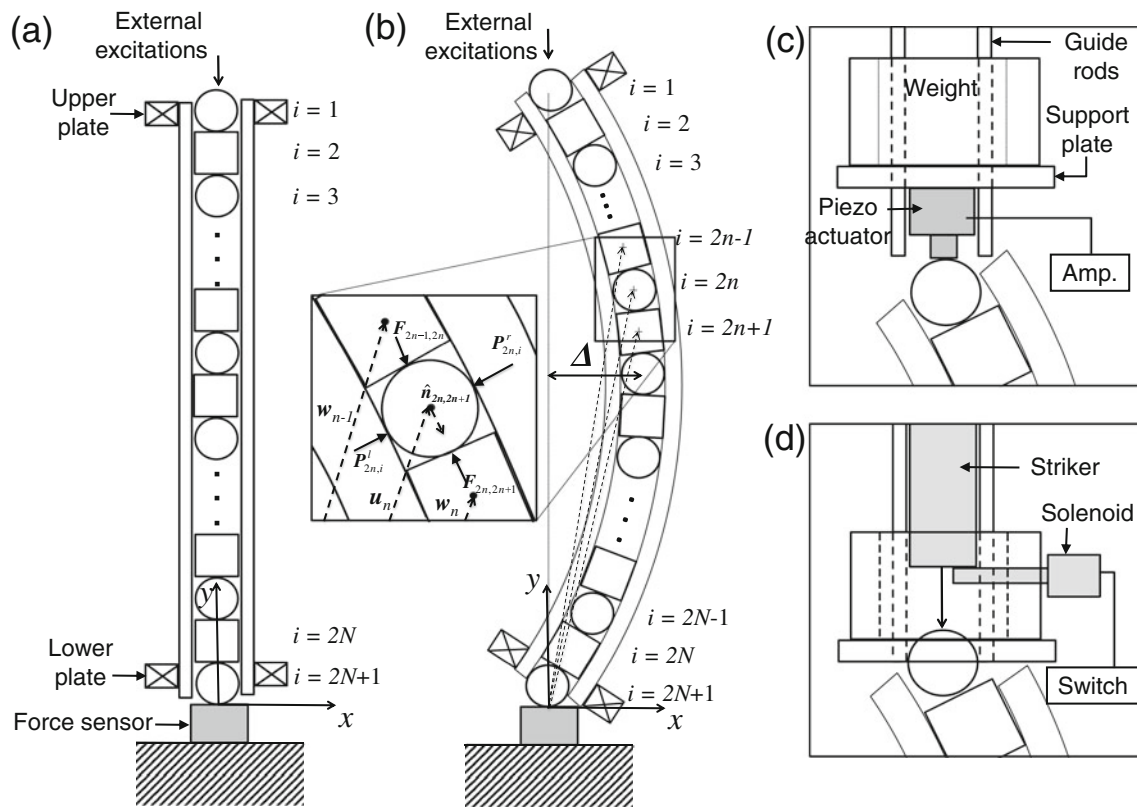


Fig. 1 Schematic of experimental setup. (a) A straight chain constrained by stainless steel guides. (b) A curved chain guided by bent PTFE guides. Inset shows a magnified view of particles under the interaction with linear guides. (c) A piezoelectric actuator to apply broadband excitations to the granular chain. (d) Striker impacts using cylindrical masses. A solenoid is used to release the striker from a designated drop height

of hardened precision steel shafts. In this straight system, the propagation of stress waves is governed primarily by the axial interactions between the granular particles excited by an impact. In the curved diatomic chain, the particles are guided by four polytetrafluoroethylene (PTFE) rods, which can flex upon the vertical impact applied to the granular chains. As a result, the transmission of waves along the granular crystals becomes affected by the coupling mechanism between the granules and the soft PTFE guides in the lateral direction. In this study the PTFE material is chosen for its flexibility and effectiveness in reducing friction during these interactions. The PTFE rods have an outer radius $R_G=6.35$ mm, density $\rho_G=4,302$ kg/m³, elastic modulus $E_G=0.46$ GPa, and Poisson's ratio $\nu_G=0.46$. The initial curvature of the chain is determined by the bent PTFE rods, which are held by the upper and lower stainless steel plates (Fig. 1(b)). We represent the curvature of the chain by Δ , which measures the offset of the chain from its centerline. In this study, we test six different configurations of curved chains ($\Delta=[22.4, 35.2, 58.9, 66.2, 73.3, 85.2]$ mm). A customized linkage structure provides vertical and rotational degrees of freedom of the upper plate upon the external impact.

To vary the profiles and magnitudes of external excitations applied to the granular chains, we use two different apparatuses: a piezoelectric actuator (Fig. 1(c)) and impact strikers (Fig. 1(d)). The piezoelectric actuator is used to apply small-amplitude disturbances to the granular chain over a wide range of frequencies. In this study, we use a commercial piezoelectric actuator (Physik Instrumente P-212) powered by an external voltage amplifier (Piezo Systems Linear Amplifier EPA-104). We condition its output with white-noise signals (1-second duration) generated by MATLAB. The piezoelectric actuator is mounted to a guided support plate to make a direct contact with the top sphere of the chain. To impose pre-compression to the granular crystal, we place a ring-shaped weight on top of this support plate. In this study, we vary the amount of pre-compression by two orders of magnitude from 4.7 N (weight of the support plate) to 306.9 N.

Using a piezoelectric actuator, the maximum amplitude of the excitation forces is limited by the stroke length of the transducer and by the power available from the external amplifier. To investigate the nonlinear responses of the granular chain using large disturbances beyond the limits of the piezoelectric transducer, we excite dynamic impacts

via striker drop (Fig. 1(d)). We use two different types of strikers: a spherical striker made of aluminum 2017-T4 (19.05-mm diameter) and a group of cylindrical strikers (440 C stainless steel) in various lengths. Using these striker impacts, we can achieve a wide range of compressive forces from ~50 N (aluminum sphere drop from 3.2 mm) to approximately 1,000 N (679 g cylinder drop from 10 mm). To control the amplitude of dynamic forces, we employ 13 different cylindrical strikers with a 9.53-mm radius and length $L=[6.35, 9.53, 12.7, 15.9, 19.1, 22.2, 25.4, 50.8, 102, 152, 203, 254, 305]$ mm. This corresponds to different strikers' mass $M=[14.1, 21.2, 28.2, 35.3, 42.3, 49.4, 56.5, 113, 226, 339, 452, 565, 678]$ g. To impact the top sphere of the chain, we release spherical and cylindrical strikers from 3.2-mm and 10-mm drop heights respectively using a DC-powered solenoid [27]. We apply pre-compression to the chain by resting a weight on the top of a guided support plate, which has a central hole to expose partially the top sphere for striker impacts. The ring-shaped weight is cut open to allow the access of the solenoid in the lateral direction.

We measure the transmitted waves through the granular chain using a commercial force sensor (Piezotronics, PCB-C04) positioned at the bottom of the granular crystal. We mount the force sensor on a massive block that simulates a rigid wall. The physical stiffness of the force sensor is 1.05×10^9 N/m, which is much higher than the contact stiffness between the diatomic particles over the range of pre-compression forces considered in this study (the maximum contact stiffness calculated is 5.96×10^7 N/m under static pre-compression 306.9 N for the straight chain). The sensor's cap is made of hardened 17-4 PH (H900) stainless steel, which is assumed to have identical density, elastic modulus, and Poisson's ratio to those of the beads composing the chain. The sensor is connected to a data acquisition board (National Instrument PCI-6115) to collect signals at a sampling frequency up to 10 MHz. For the statistical treatment of signals, we average the measurements over five acquisitions, and the acquired signals are processed in MATLAB.

Theoretical Background and Numerical Approach

Previous studies have shown that a 1D granular crystal can be modeled as a chain of point masses connected by nonlinear springs based on Hertzian law [2, 5]. The numerical approach using this discrete element (DE) model is valid if the particles' interactions are restricted to small displacements and if the transit times of the stress waves in the granular crystal are much longer than the oscillation period of elastic waves within the

particles [2]. Using this DE model, we can express the equations of motion for the diatomic particles in a curved chain as:

$$\begin{aligned} m_s \ddot{\mathbf{u}}_n &= \mathbf{F}_{2n-1,2n} + \mathbf{F}_{2n,2n+1} + \mathbf{P}_{2n}^l + \mathbf{P}_{2n}^r + m_s \mathbf{g} \\ m_c \ddot{\mathbf{w}}_n &= \mathbf{F}_{2n,2n+1} + \mathbf{F}_{2n+1,2(n+1)} + \mathbf{P}_{2n+1}^l + \mathbf{P}_{2n+1}^r + m_c \mathbf{g}, \end{aligned} \quad (1)$$

where m_s and m_c are the masses of a sphere and a cylinder, \mathbf{u}_n and \mathbf{w}_n are the position vectors to their centers in the n -th unit cell, and \mathbf{g} is the gravitational constant (see the inset in Fig. 1(b)). The axial force $\mathbf{F}_{2n,2n+1}$ exerted on the $2n$ -th particle by the neighboring $(2n+1)$ -th particle can be expressed as:

$$\mathbf{F}_{2n,2n+1} = A[D - |\mathbf{u}_n - \mathbf{w}_n|]_+^k \hat{\mathbf{n}}_{2n,2n+1}, \quad (2)$$

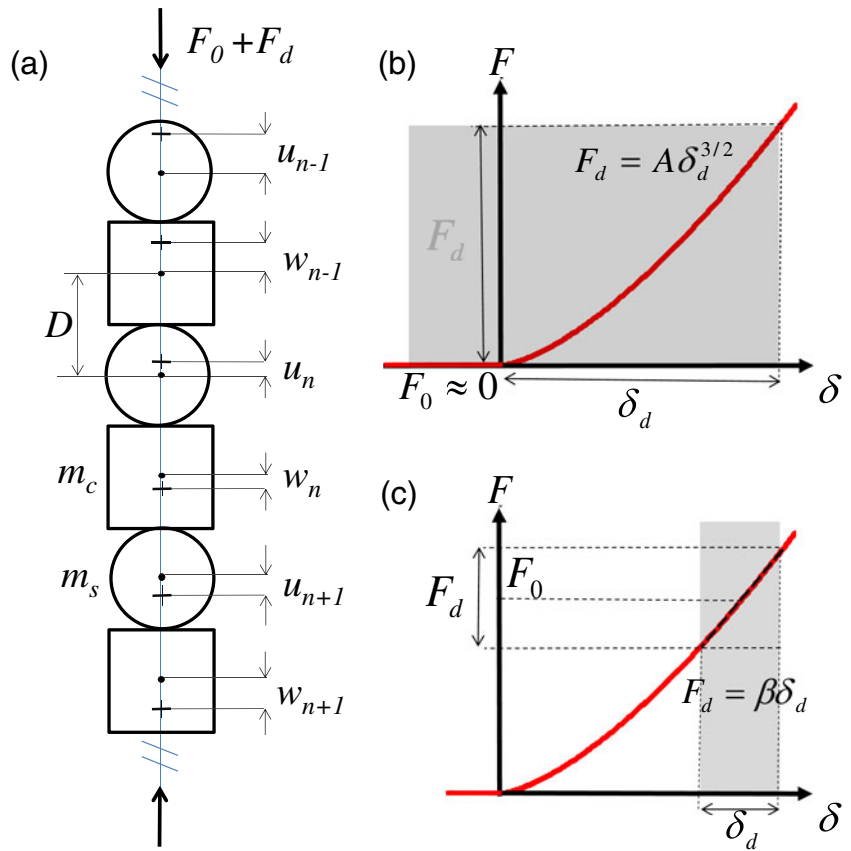
according to the Hertzian contact law. Here the unit cell length is D , and the bracket $[x]_+$ takes only positive values and returns 0 if $x < 0$, implying no tensile strength between particles. The unit normal vector $\hat{\mathbf{n}}_{2n,2n+1}$ is defined as $\hat{\mathbf{n}}_{2n,2n+1} = (\mathbf{u}_n - \mathbf{w}_n) / |\mathbf{u}_n - \mathbf{w}_n|$. Given the configurations of the sphere-cylinder contact, the Hertzian factor is $k=3/2$ and the coefficient A can be derived as $A = \frac{4\sqrt{R_c}}{3} \left(\frac{1-\nu_s^2}{E_s} + \frac{1-\nu_c^2}{E_c} \right)^{-1}$. Here, R , E , and ν represent the radius, elastic modulus, and Poisson's ratio of particles with the subscript s and c denoting spherical and cylindrical elements [28]. Note that the particle distance D and the Hertzian coefficient A in (equation (2)) need to be modified at the end of the granular chain, such as the interface with the elastic half space and the striker, to account for the bounding medium's material and geometrical condition [27]. The lateral interactions with the right- and left-hand guiding media, \mathbf{P}_{2n}^r and \mathbf{P}_{2n}^l can be also expressed using the modified Hertzian contact law. For the sake of brevity, we do not include the expressions of the lateral contact forces in this manuscript. The complete descriptions of the axial and lateral forces including dissipative terms can be found in [26].

We simplify the equations of particles' motion into a one-dimensional form for theoretical considerations, while we tackle the two-dimensional (equation (1)) for numerical integrations. After neglecting the lateral forces and the gravitational effect, (equation (1)) becomes:

$$\begin{aligned} m_s \ddot{u}_n &= A(w_{n-1} - u_n)_+^k - A(u_n - w_n)_+^k \\ m_c \ddot{w}_n &= A(u_n - w_n)_+^k - A(w_n - u_{n+1})_+^k. \end{aligned} \quad (3)$$

Here, w and u are the displacements of cylindrical and spherical particles from their equilibrium positions (Fig. 2 (a)), which should not be confused with the location vectors of particles in (equation (1)). Depending on the level of nonlinearity in the granular system, (equation (3)) can be approximated into different mathematical forms, thereby producing distinctive sets of mathematical solutions. Physically, these solutions correspond to different types of stress

Fig. 2 (a) Schematic of a one-dimensional granular chain composed of spherical and cylindrical elements. (b) The force-displacement diagram of Hertzian nonlinear contact. A highlighted region in gray color represents a fully nonlinear regime under large disturbances relative to the static pre-compression. (c) Force-displacement diagram under the linear approximation. Given small disturbances compared to pre-compression, the force-displacement relationship can be linearized as shown with a dashed line in the highlighted region



waves ranging from linear elastic waves to highly nonlinear solitary waves that can be generated and propagated in a diatomic chain.

Highly Nonlinear Regime

In a highly nonlinear regime, the interactions of granular particles are governed by a full range of Hertzian nonlinear contact (Fig. 2(b)). In this configuration, the amplitude of dynamic disturbances (F_d) applied to the granular chain is much larger than that of the static pre-compression (F_0). Given such a high-level nonlinearity, Porter et al. derived a closed-form solution of (equation (3)) using the long-wave approximation to describe wave dynamics in a general one-dimensional diatomic chain [29]. We briefly introduce the analytical process of the closed-form solution derivation, while details can be found in [29, 30].

Under the assumption of acoustic-mode excitations (i.e., in-phase oscillations of diatomic particles in a unit cell), the displacement of a cylindrical particle can be approximated in terms of the neighboring spherical particle’s motion by a Taylor expansion up to the fourth order [29, 30]:

$$w \cong u + b_1 D u_x + b_2 D^2 u_{xx} + b_3 D^3 u_{xxx} + b_4 D^4 u_{xxxx}. \quad (4)$$

Here, D denotes the distance between two particles in a unit cell, and the coefficients are found to be $b_1=1$, $b_2=m_s/(m_s+m_c)$, $b_3=(2m_s - m_c)/3(m_s+m_c)$, and $b_4=m_s(2m_s^2 - m_s m_c + m_c^2)/3(m_s+m_c)^3$ [30]. After plugging this into (equation (3)) and incorporating terms, it is possible to obtain a differential equation in the following form [29, 30]:

$$u_{\tau\tau} = u_x^{k-1} u_{\tau\tau} + G u_x^{k-3} u_{xx}^3 + H u_x^{k-2} u_{xx} u_{xxx} + I u_x^{k-1} u_{xxxx}, \quad (5)$$

where $\tau = t\sqrt{2kD^{k+1}/(m_s + m_c)}$ is a rescaled time. The constants in (equation (5)) are $G=D^2(2-3k+k^2)m_s^2/6(m_s+m_c)^2$, $H=D^2(k-1)(2m_s-m_c)/3(m_s+m_c)$, and $I=D^2(m_s^2 - m_s m_c + m_c^2)/3(m_s+m_c)^2$ [29, 30]. This equation is fundamentally similar to the differential equation that Nesterenko derived to describe the dynamics of a uniform spherical chain [2].

After several algebraic steps, an exact solution of (equation (5)) can be obtained in the highly nonlinear regime, i.e., when the pre-compression applied to the granular chain is significantly smaller than the dynamic

disturbances ($F_d \gg F_0$). The trigonometric solution can be expressed as [29, 30]:

$$u_\xi = B \cos^{2/(k-1)}(\alpha \xi), \quad -\frac{\pi}{2} \leq \alpha \xi \leq \frac{\pi}{2}, \quad (6)$$

where ξ is a rescaled strain in the homogenized granular system, B is a parameter dependent on the wave speed and material properties, and α is a coefficient determined by mass-ratios (m_s/m_c) of the diatomic granular system. The solution of the nonlinear equation (3) is a single arch of the periodic profile as represented in (equation (6)), implying a finite-width wavelength of the nonlinear waves formed in the granular system [30]. For a monodispersed chain composed of spherical particles, Nesterenko found that the spatial width of the propagating waves is equivalent to approximately five-particle diameters [2]. For a diatomic granular chain, the shape and propagating properties of nonlinear waves depend on the combination of the materials and mass-ratios of particles that compose the chain [29, 30]. New families of solitary waves in dimer chains have also been presented in [31].

Linear Regime

Now we examine the propagation of acoustic waves when a granular chain is strongly compressed relative to the amplitude of the dynamic disturbances ($F_d \ll F_0$) (Fig. 2(c)). In this case, we can separate the displacements of particles into static and dynamic components as $u_n = u_{n,sta} + u_{n,dyn}$ and $w_n = w_{n,sta} + w_{n,dyn}$, where subscript ‘*sta*’ and ‘*dyn*’ denote static and dynamic elements. We can plug these into (equation (3)) and expand it using the Taylor series under the assumption that the static displacement is much larger than the dynamic one. Neglecting the dynamic displacement terms of the second and higher order, we obtain a linearized equation of motion as [24]:

$$\begin{aligned} m_s \ddot{u}_{n,dyn} &= \beta(w_{n-1,dyn} - u_{n,dyn}) - \beta(u_{n,dyn} - w_{n,dyn}) \\ m_c \ddot{w}_{n,dyn} &= \beta(u_{n,dyn} - w_{n,dyn}) - \beta(w_{n,dyn} - u_{n+1,dyn}). \end{aligned} \quad (7)$$

Here, the static displacement components are cancelled out due to the force equilibrium and thus, the equation of motion is described solely in terms of dynamic disturbances. However, it should be noted that a linearized stiffness β is determined by the static compression as:

$$\beta = \frac{3}{2} A^{2/3} F_0^{1/3}, \quad (8)$$

where F_0 denotes the static pre-compression force initially applied to the granular crystal. This implies that larger pre-compression yields higher stiffness between the adjoined particles.

We analytically solve (equation (7)) under the assumption that there is no dissipation in the system and that the chain is infinitely long (i.e., there is no loss of energy and no boundary effects). We use the Floquet’s principle in which the particle dynamics in a given cell is assumed to be fundamentally identical to that of its neighboring cell based on the periodicity of the system [32, 33]. Mathematically, this implies that the particles’ motion in the $(n+1)$ -th cell is expressed as $u_{n+1,dyn}(t) = u_{n,dyn}(t) e^{-i(4\pi D/\lambda)}$ and $w_{n+1,dyn}(t) = w_{n,dyn}(t) e^{-i(4\pi D/\lambda)}$, where λ is the wavelength of the propagating waves and $u_{n,dyn}(t)$ and $w_{n,dyn}(t)$ are the dynamic displacements of particles in a reference (i.e., n -th) cell. After substituting these periodic expressions into (equation (7)) and imposing the condition of non-trivial solution, we obtain the following characteristic equation defining the dispersive relation [24]:

$$m_s m_c \omega^4 - 2\beta(m_s + m_c)\omega^4 + 2\beta^2(1 - \cos(4\pi D/\lambda)) = 0, \quad (9)$$

where ω is the angular frequency. By solving (equation (9)), we obtain the dispersion curve that defines the angular frequencies of the propagating waves as a function of their wavelengths (see Fig. 3 for $F_0 =$

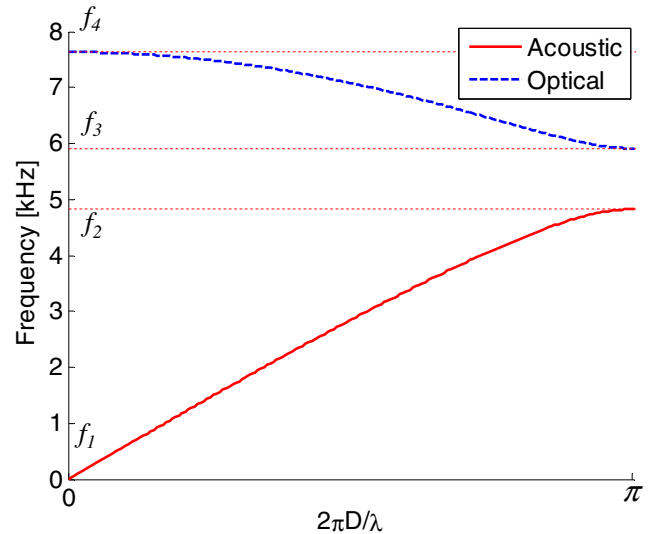


Fig. 3 Dispersion diagram of a diatomic granular chain. The lower and upper curves represent acoustic and optical pass bands respectively. A band-gap is formed between two distinctive pass bands. The cutoff frequencies are $[f_1, f_2, f_3, f_4] = [0, 4.827, 5.911, 7.632]$ kHz, given the 10 N pre-compression



10 N). In this dispersion curve, the cutoff frequencies of this dispersion relationship are found at $\lambda = 2D$ and $\lambda = \infty$:

$$f_1 = 0, \quad f_2 = \frac{1}{2\pi} \sqrt{\frac{2\beta}{m_c}}, \quad f_3 = \frac{1}{2\pi} \sqrt{\frac{2\beta}{m_s}},$$

$$f_4 = \frac{1}{2\pi} \sqrt{\frac{2\beta(m_s + m_c)}{m_s m_c}}. \quad (10)$$

It is evident that a 1D granular crystal in the linear regime allows the propagation of waves only in certain frequency ranges [24]. The allowable frequency bands in $[f_1, f_2]$ and $[f_3, f_4]$ are called acoustic and optical bands, respectively. The stress waves whose frequencies belong to the frequency band in $[f_2, f_3]$ cannot propagate in the granular system. These forbidden frequency bands are referred to as band-gaps or stop bands. The cutoff frequencies in (equation (10)) are functions of the particle masses and of the linearized stiffness β . As described in (equation (8)), β can be altered by simple manipulation of the pre-compression applied to the granular system. This means that the acoustic structure of diatomic granular crystals can be tuned *in situ* without changing materials or geometry of unit cell particles [24, 25].

The theoretical aspects of wave propagation in curved granular crystals are not as simple as those in a straight chain, due to the complex coupling mechanism between the granular and elastic media. To calculate the particles' dynamics in a curved chain and their interactions with soft elastic guides, we employ a numerical method that combines a discrete element (DE) and a finite element (FE) model. The DE model simulates the two-dimensional interactions of granular particles based on the Cundall [34] and Tsuji [35] models, which are built on the classical Hertz-Mindlin theory [28]. The dynamics of linear elastic guides are calculated by the FE model that discretizes the linear elastic guides into the Bernoulli-Euler beam elements [36]. The combined DE and FE model takes into account the axial and tangential interactions among particles, including dissipative terms. In this study, we suppress the dissipative terms among particles to assess the wave attenuation solely contributed by the structural coupling between granules and the linear elastic guides. The details of the combined DE and FE model can be found in [26].

Results and Discussion

In this section, we present the experimental and numerical results obtained by varying the static pre-compression, the chain curvatures, and the impact amplitude via different striker masses. We compare these results with the theoretical predictions and discuss the findings.

Pre-Compression Effect

We begin investigating the effect of pre-compression on the propagation of stress waves in granular crystals. We excite the straight granular chain (Fig. 1(a)) using a spherical aluminum striker and measure the transmitted waves arriving in the force sensor under various pre-compressions applied to the chain. Figure 4(a) reports selected force profiles that are experimentally measured all under the identical striker impact conditions. To ease graphical illustration, the results are plotted with a vertical shift of 50 N. Here, the positive components in the y-axis denote compressive force, while the negative components represent tensile forces. The time in the x-axis is measured with respect to the trigger of the sensor at $t=0.4$ ms, when the force amplitude reaches a threshold level. In Fig. 4(a), the lowest curve shows a force-time history obtained from a straight chain under no pre-compression, in which the dynamic disturbances are dominant in comparison to the pre-compression. In this configuration, we expect the propagation of highly nonlinear solitary waves, as evident in the experimental measurement by the presence of a single pulse appearing around a time $t \sim 0.5$ ms. We also observe small-amplitude fluctuations following this impulse, which are likely caused by the oscillations of the particles within a unit cell. This differs from a clean, single hump of compressive waves witnessed in a monodispersed granular chain [2].

The nonlinear waves under zero-precompression are attributed to the highly nonlinear interactions between the particles as discussed in Section III. As the pre-compression increases relative to the dynamic disturbances, the interfacial stiffness between the particles transits from nonlinear to linear relationship, which yields an approximately uniform interfacial stiffness value between particles. In other words, the granular architecture becomes similar to a linear lattice structure, which supports the propagation of linear elastic waves. As a result, under the large values of pre-compression, we find that the transmitted waves are highly oscillatory, showing the propagation of not only compressive forces but also tensile components among the particles (Fig. 4(a)). Note that these tensile forces in the compressed chain do not imply the separation of particles, since the magnitude of pre-compression is much larger than the dynamic forces ($F_d/F_0 \approx 0.1$ for $F_0=307$ N) and all particles remain compressed in contact with each other. The oscillatory waves observed in the strongly pre-compressed chains are caused by the propagation of particles' vibration (also called phonon) in linear lattices. This is fundamentally different from highly nonlinear solitary waves deriving from the unidirectional compressive motions of particles under zero pre-compression and no tensile strength. This is why uncompressed granular crystals are sometimes referred to as "sonic vacuum" due to their incapability of transmitting linear elastic waves [2].

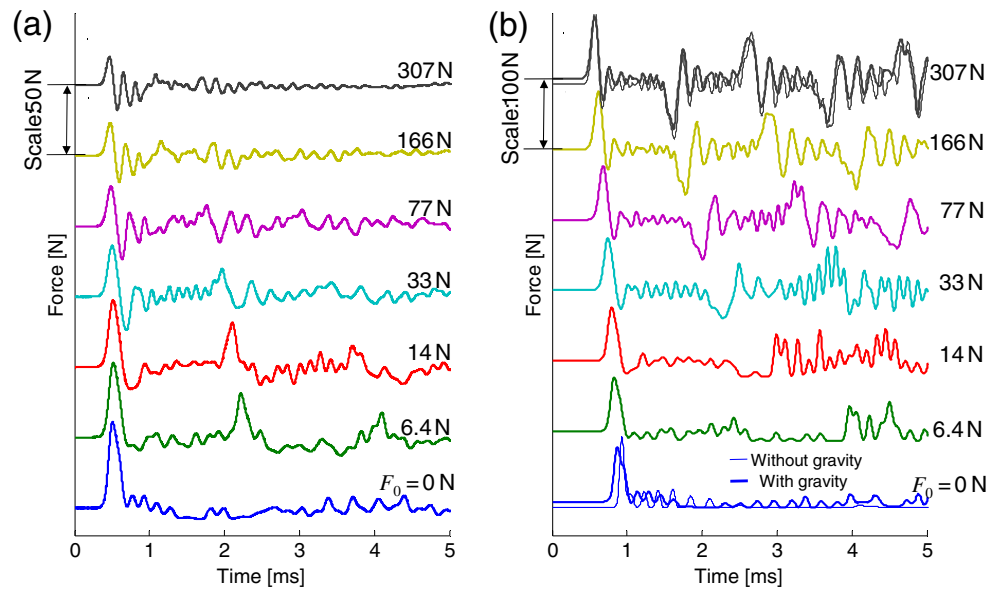


Fig. 4 (a) Experimental and (b) Numerical force profiles of transmitted waves through the diatomic granular chain under various pre-compressions. To ease visualization, the experimental and numerical force profiles are plotted with vertical shifts of 50 N and 100 N, respectively. The force profile positioned at the top shows oscillatory mechanical waves under high pre-compression (307 N), whereas the bottom curve corresponds to compactly-supported solitary waves under no pre-compression (0 N). The numerical force profiles under $F_0=0$ and 307 N (top and bottom curves in (b)) also include the simulation results without gravitational effects (*thinner lines*) on the top of those under gravity (*thicker lines*)

The numerical results are reported in Fig. 4(b), in which a time $t=0$ ms denotes the moment that the striker collides with the top particle in the chain. We find that they corroborate the experimental results. However, the amplitude of the numerical force profiles is larger than that of the experimental measurements. Such a discrepancy stems from the absence of dissipative effects in the numerical simulations. Dissipative mechanisms in granular crystals have been studied previously, including the authors' work based on empirical Laplacian model [37] and quasi-static model using a Hertz-Mindlin theory [26]. However, these models are primarily focused on the attenuation of solitary waves in a 1D granular chain, while they are not properly applicable to the strongly compressed chain. Despite the negligence of the dissipative effects, however, we find that the DE-FE model successfully predicts the transition of wave characteristics from nonlinear to linear modes. From the numerical simulation results in Fig. 4(b), it is evident that the speed of the transmitted waves is faster as the amplitude of the static pre-compression increases. Such amplitude-dependence of wave speed is a unique property of general types of nonlinear waves observed in a variety of physical systems [2, 38–41].

It is also worth discussing the effect of gravity, given the chain's vertical configuration in this study. To investigate the gravitational effect, we calculate the transmitted wave profiles with and without the inclusion of gravity, when there is no external pre-compression ($F_0=0$). Comparing

the thick (gravity) and thin (no gravity) curves at the bottom of Fig. 4(b), we find that the gravitational effect is noticeable in terms of wave form and speed. Particularly, the force profile under the gravitational effect contains more oscillatory components of stress waves compared to that without gravity. The offset between the two curves at the beginning of the signals corresponds to the weight of the granular chain that amounts to 7.7 N. However, the amount of compressive force induced by the chain weight is yet an order of magnitude smaller than the dynamic disturbances caused by the striker drop ($F_d/F_0 \approx 11.0$). Therefore, the qualitative nature of the propagating waves remains the same, exhibiting highly nonlinear solitary wave shapes. Figure 4(b) also includes a simulated result of the gravitational effect under the maximum pre-compression ($F_0=307$). In this strongly compressed granular chain, the effect of gravity is even more insignificant as comparing the two curves in the top of Fig. 4(b). This is because the gravity-induced force is very small relative to the externally imposed compression. Therefore, the oscillatory shapes of the propagating waves are similar, and the change of cutoff frequency of the propagating waves is expected to be negligible, considering $f_c \propto F_0^{1/6}$ deduced from (equations (8) and (10)) (cutoff frequency shift is $\sim 0.4\%$ due to gravity when $F_0=307$).

To investigate the frequency spectrum of the transmitted waves, we perform a fast Fourier transform (FFT) of the measured time-domain signals. As a result, Figure 5(a) shows an experimental plot of the power spectral density (PSD) in a

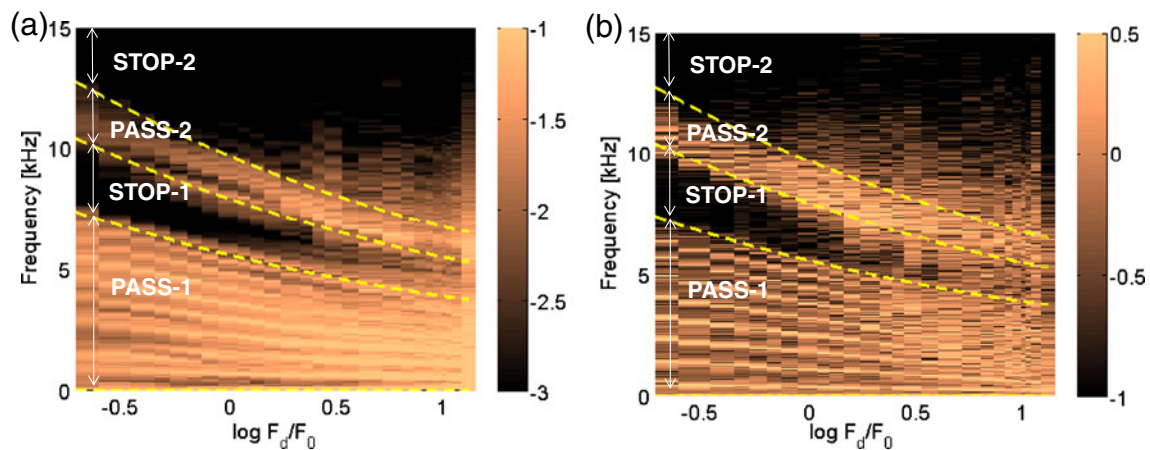


Fig. 5 (a) Experimental and (b) numerical results of PSD in a diatomic band structure as a function of F_d/F_0 . The highlighted zones represent pass bands, while dark zones correspond to band gaps. The color bars denote transmission gains in a logarithmic scale. Yellow dotted lines denote cutoff frequencies based on theoretical dispersion relationship

logarithmic scale, as a function of the static preload and frequency. Here, the light color regions represent the high amplitude ratios of transmitted waves to the input excitations (also called transfer function gain) (see the color bar in Fig. 5(a)). The dashed lines correspond to the theoretical cutoff frequencies in the dispersion relation, obtained from (equation (10)). The abscissa of the figure denotes the level of system nonlinearity quantified by the ratio of the dynamic disturbances to the static pre-compression (F_d/F_0). Since the dynamic disturbances are identical throughout the experiments, the variations of F_d/F_0 are solely determined by the pre-compression effect. The ordinate represents the frequency components of the transmitted waves.

We note that frequency band structures are formed with distinctive pass- and stop-bands, whose frequency ranges vary sensitively with the amount of static pre-compression. This is consistent with the analytical prediction that a diatomic granular crystal forms acoustic and optical pass-bands and that their cutoff frequencies are governed by the linearized stiffness β , which in turn is a function of the chain pre-compression [24]. In Fig. 5(a), the acoustic and optical frequency bands are denoted as ‘pass-1’ and ‘pass-2’. The stop band positioned between two pass-bands is denoted as ‘stop-1’, and we conventionally refer to the forbidden band located above the optical band as the ‘stop-2’ band. We find that our experimental results are in agreement with the theoretical prediction.

Another interesting point is the dependence of transmission gains (i.e., PSD values) on F_d/F_0 . In Fig. 5(a), the differences of PSD values between pass- and stop-bands are obvious in the lower F_d/F_0 , while such distinction become less evident in the higher F_d/F_0 . This translates into the fact that the classical frequency band structure is a characteristic of the linear regime, with small-amplitude dynamic disturbances relative to the pre-compression (i.e., small F_d/F_0). In the case of zero or weak pre-compression (rightmost data sets in Fig. 5(a)), we observe the concentration of PSD values in the low frequency

regime, but it is hard to distinguish pass- and stop-bands within this region. Figure 5(b) shows the corresponding numerical results based on the DE model.

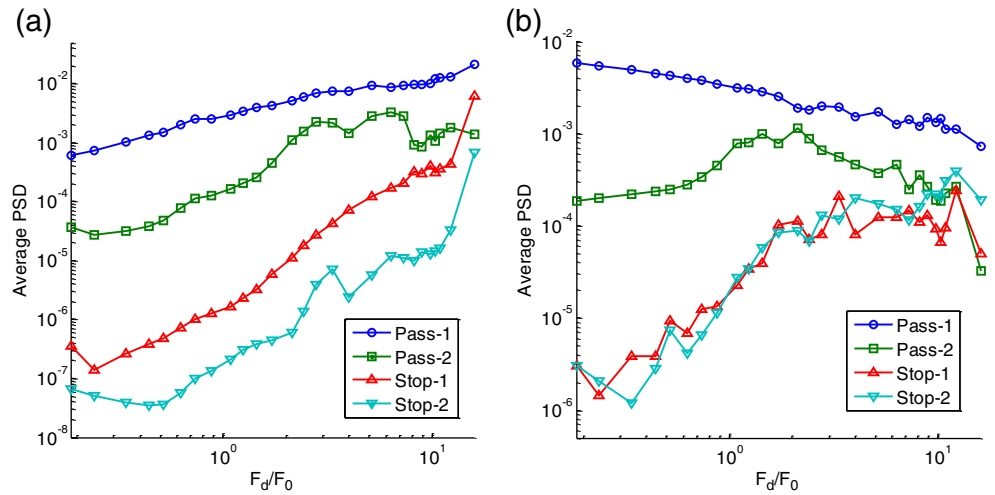
To analyze the evolution of the frequency band structures, we calculate the average PSD values in the pass- and stop-bands over a range of F_d/F_0 tested in this study. Mathematically, the average PSD can be quantified by:

$$\overline{PSD} = \left[\frac{1}{f_u - f_l} \int_{f_l}^{f_u} PSD^2 df \right]^{1/2}, \quad (11)$$

where f_l and f_u are the cutoff frequencies corresponding to the lower and the upper boundaries of the frequency band. This value represents the amount of energy transmitted in the given frequency band normalized by the width of the frequency bands. Figures 6(a) and (b) show the experimental and numerical results of the average PSD values as a function of the nonlinearity level (F_d/F_0). We find that the average PSD values in pass-bands are significantly higher than those in the stop-bands in the linear regime (i.e., low F_d/F_0). However, the discrepancies between pass- and stop-bands are reduced as the nonlinearity level is increased (i.e., high F_d/F_0). In particular, the average PSD values of the stop-bands become equivalent to those of the pass-bands at the maximum nonlinearity level. The experimental and numerical results are qualitatively in agreement.

We quantify the prominence of frequency band structures by calculating the ratios of pass-band PSD values to those of the neighboring stop-bands (Fig. 7). Here, the blue curve with circular marks represents the PSD ratios of the first pass- and stop-bands (Pass-1/Stop-1), while the green curve with rectangular marks denotes the PSD ratios of the second pass- and stop-bands (Pass-2/Stop-2). We find that at a low F_d/F_0 , the PSD ratio is as high as $10^3 \sim 10^4$ due to the obvious dispersion of propagating waves and the resulting

Fig. 6 Average PSD values as a function of nonlinearity levels (F_d/F_0). Four curves represent the PSD values calculated in pass- and stop-bands formed in a diatomic granular chain. **(a)** Experimental results. **(b)** Numerical results



formation of frequency band structures. However, as the degree of nonlinearity increases, the PSD ratios decrease to the level of $10^{-1} \sim 10^1$, which suggests the disappearance of the frequency band structures. The experimental and numerical results are in agreement. The observed trend proves that the frequency band structure becomes dominant only if the granular system supports the propagation of linear elastic waves with intrinsic dispersive characteristics. As a granular chain is excited by strong excitations and starts to form nonlinear waves, the transmitted waves no longer contain frequency components that correspond to the acoustic and optical pass bands.

Chain Curvature Effect

In this section, we discuss the effects of the chain’s curvature on the formation of frequency band structures. We excite the granular crystals using a piezoelectric actuator to consistently apply small-amplitude, wide-band signals in a controllable manner. The maximum amplitude of the dynamic disturbances is limited to 0.5 N, which is orders of

magnitude smaller than the static pre-compression used in this study [$F_0 = 56.4$ N, $Order(F_d/F_0) \approx 10^{-2}$]. For numerical simulations, we use the same order of F_d/F_0 to allow the formation of a full-fledged frequency band structure.

Figure 8 reports the frequency spectra of stress waves transmitted through diatomic chains with four different curvatures. The y-axis is in a logarithmic scale, and the signals are shifted by 10^2 to ease visualization. The black vertical dashed lines represent analytic predictions of cutoff frequencies from (equation (10)) for an equivalent straight chain ($\Delta = 0$). Given the amplitude of the pre-compression used in experiments, we obtain cutoff frequencies at $f_1 = 0$ kHz, $f_2 = 6.46$ kHz, $f_3 = 7.91$ kHz, and $f_4 = 10.2$ kHz. From the experimental results in Fig. 8(a), we observe the presence of both acoustic and optical bands depicted by the shaded regions in the left- and right-hand sides (i.e., ‘pass-1’ and ‘pass-2’). These pass-bands are characterized by the sharp spikes representing the resonant frequencies supported by the finite diatomic chains. In the straight chain, the measured pass bands agree well with the theoretically predicted cutoff frequencies (top blue curve and vertical dashed lines in

Fig. 7 The average PSD ratios of pass-bands to their adjacent stop-bands. **(a)** Experimental results. **(b)** Numerical results

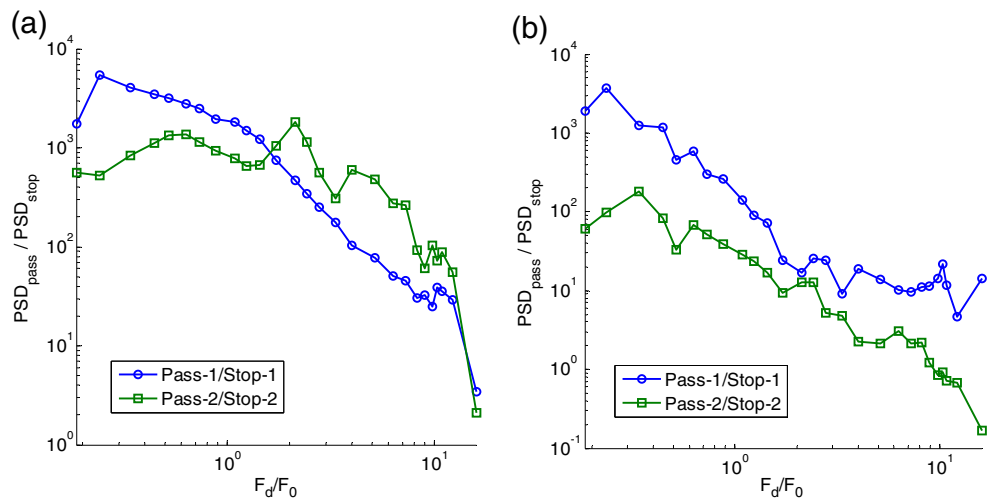


Fig. 8 PSD of transmitted waves for the curved chain with $\Delta=[0, 35.2, 66.2, 85.2]$ mm. **(a)** Experimental results. **(b)** Numerical results. The shaded regions in the left- and right-hand sides represent the acoustic and optical pass-bands

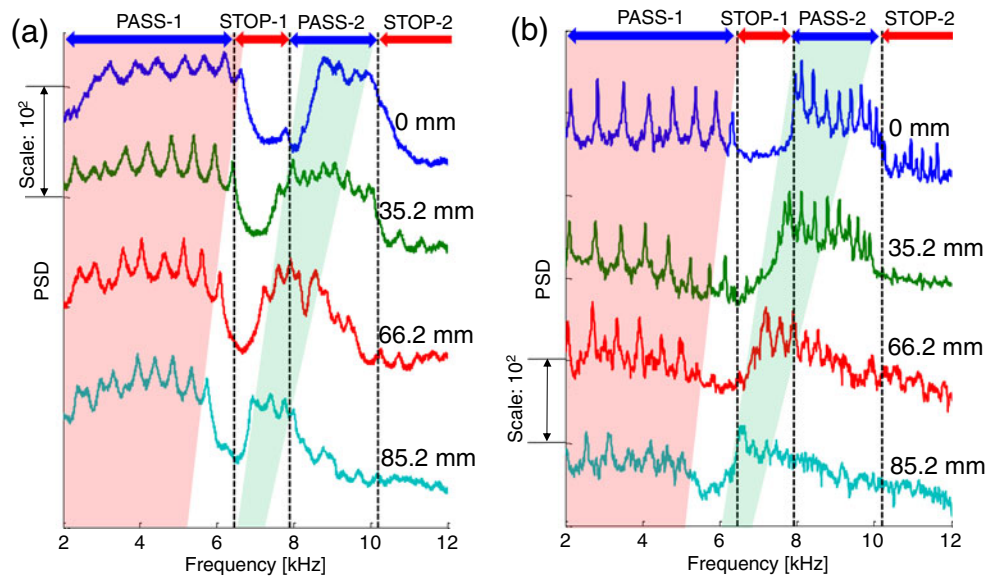


Fig. 8(a)). In curved chains, however, we find frequency bands gradually down-shifting as the chain curvature increases. In particular, when the chain's curvature becomes 85.2 mm (bottom cyan curve in Fig. 8(a)), the optical pass band shifts to the middle of band-gap predicted for a straight chain. The numerical results in Fig. 8(b) corroborate the experimental results.

To show the evolution of frequency bands as a function of the chain curvature, we report in Fig. 9 the surface maps corresponding to the experimental and numerical results shown in Fig. 8. We plot the experimental results from seven different curvatures ($\Delta=[0, 22.4, 35.2, 58.9, 66.2, 73.3, 85.2]$ mm) in Fig. 9(a), and we present the shift of frequency bands obtained numerically for every 5-mm offset from $\Delta=0$ mm to 100 mm in Fig. 9(b). Here, the horizontal dashed yellow lines denote the analytic cutoff frequencies of acoustic and optical pass bands for the straight chain. In Fig. 9(a)

and (b), the upper bright band corresponds to the optical pass band, while the lower bright band denotes the acoustic pass band. The presence of a stop band between the optical and acoustic bands is evident in both experimental and numerical results. We can also verify that the frequency bands shift towards a lower frequency zone as the curved chain exhibits a larger curvature. In particular, the shift of the optical pass band is more drastic than that of the acoustic band.

We can qualitatively explain the dependence of frequency band structures on the chain's curvature by assessing the static compression between granules in a curved chain: From the force equilibrium when an identical static load is applied to the granular chains, the compressive force between granules is decreased as the chain's curvature is increased. This is because a curved chain dispenses a portion of compressive force to the guides through lateral

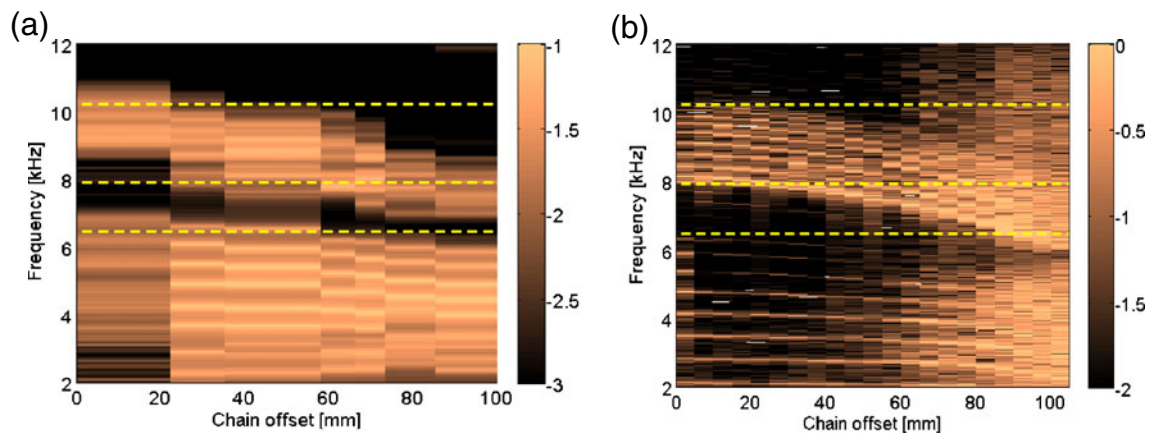


Fig. 9 Surface maps of PSD as a function of diatomic chain curvature represented by chain offset values. **(a)** Experimental results for $\Delta=[0, 22.4, 35.2, 58.9, 66.2, 73.3, 85.2]$ mm. **(b)** Numerical results for the various curvatures. The color bar reports the ratio of transmitted-wave amplitudes to those of input excitations in a logarithmic scale. Dashed yellow lines denote cutoff frequencies of acoustic and optical pass bands

contact, while all compressive loading is imposed on the granular particles in the case of a straight chain. Thus, despite the identical pre-compression applied to the chain, the granules in a curved chain are less compressed than those in a straight chain. According to the calculation of the linearized stiffness in (equation (8)), a reduced amount of compression between the particles produces a smaller stiffness value, which leads to the decreased cutoff frequencies. Consequently, we observe a down-shifting of frequency bands as we apply a larger offset to a curved granular chain. This means that compared to the straight chain, it is possible to obtain an additional parameter to control the frequency response of a curved chain by leveraging the coupling mechanism between the granules and the guided structures.

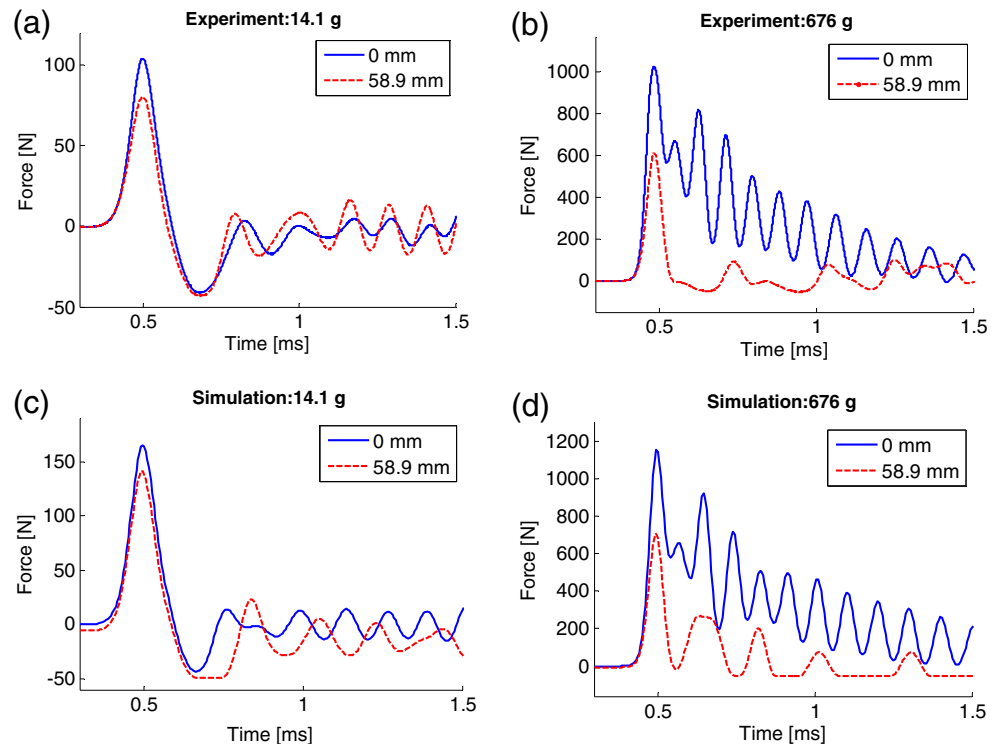
Striker Mass Effect

In this section, we study the combined effects of both nonlinearity and geometry by impacting curved granular chains with cylindrical strikers. We control the level of nonlinearity in the system, not by changing the pre-compression (F_0), but by generating different dynamic force amplitudes (F_d) varying the striker masses. The pre-compression in these tests is kept constant at $F_0=56.4$ N. Using various combinations of strikers and chain's curvatures, we characterize the dynamic responses of the bent granular crystals focusing on the amplitude-dependent behavior of the combined granular and linear elastic media.

We first investigate the propagation of stress waves excited by a light mass striker ($M=14.1$ g) with a velocity of 0.443 m/s. The temporal force profiles recorded by the force sensor are reported in Fig. 10(a) for the straight chain (solid blue line) and the curved chain with $\Delta=58.9$ mm (dashed red line). For this light striker with a mass smaller than that of a bead ($m=28.2$ g), we find that both the straight and the curved chains result in the formation of stress waves containing both compressive (positive) and tensile (negative) components. We also observe that the initial pulses are followed by small amplitude oscillatory waves. The maximum amplitude of the leading compressive wave is approximately 100 N, which is in the same order of the static pre-compression applied to the structure. This corresponds to a weakly-nonlinear regime, characterized by the presence of leading solitary wave-like pulses followed by oscillatory waves. Comparing the responses from the straight and curved chains, we observe that the waves triggered by the light striker in the curved chain are very similar to those in the straight chain. This implies the wave transmission behaviors of the straight and curved chains are qualitatively similar in the weakly nonlinear regime. However, the maximum force measured in the curved chain is reduced by 22.9 % as compared to the straight chain (from 104 N in the straight chain to 80.2 N in the curved one). This is due to the loss of axial force components among the granules by interacting with the linear elastic guides in lateral direction.

We then characterize the wave propagation through the straight and curved chains excited by a larger mass striker

Fig. 10 Experimental results of the force-time profiles for (a) light-mass (14.1 g) and (b) heavy-mass (678 g) impacts, measured by the force sensor located at the base of the granular chains. Solid blue lines represent the measurements from the straight chain, while dotted red lines denote those from the curved chain with an initial curvature $\Delta=58.9$ mm. Numerical results are plotted for (c) light-mass and (d) heavy-mass impacts



($M=678$ g). In Fig. 10(b), we observe that the maximum force induced by the striker is in the range of $F_d \approx 1,000$ N. Note that according to [28], the maximum contact pressure developed in the system remains below plastic limit even under the heaviest striker impact. Therefore, the measured force profiles are not significantly affected by plastic effects. The maximum dynamic force is much larger than the static pre-compression applied to the chain ($F_0=56.4$ N). This implies that the chain is now under the highly-nonlinear regime. In particular, we find that the shape of the nonlinear waves propagating in the chain is totally different from that of the weakly-nonlinear waves observed in the case of the light mass impact. For the straight chain, we now observe the generation of solitary wave trains characterized by a leading pulse in large amplitude and the trailing waves decaying exponentially. The mechanism behind the formation of the solitary wave trains can be explained by the multiple collisions between the heavy-mass striker and the granular chain during the impact [8, 16, 42].

It is notable in Fig. 10(b) that the transmitted waves in the straight and curved chains present a remarkably different behavior. We find that the transmitted waves in the curved chain results in faster decay than that in the straight chain, such that no significant waves are observed after the initial impulse around 0.5 ms. The maximum amplitude of this initial pulse is also reduced by 40.3 %, from 1,027 N in the straight chain to 613 N in the curved one (see Fig. 10(b)). Considering that the area under the force-time curve corresponds to the amount of impulse transferred, we find that the transferred impulse in the curved chain is a mere 20.2 % compared to that in the straight chain. This means that the curved systems can attenuate large-amplitude impacts more effectively relative to the straight chains. Furthermore, we can observe an amplitude-dependent behavior of the curved granular chains, in which the energy absorption by the elastic guides is facilitated under stronger impacts compared to the small-amplitude disturbances. Figures 10(c) and (d) show the numerical results of the transmitted waves under the small- and large-amplitude impact. We find that the numerical results agree well with the experimental findings.

The amplitude-dependent behavior of the curved granular system can be explained by the coupling mechanism between the granules and the surrounding elastic media. While a straight chain transmits impact energy without significant losses, a curved chain dispenses the kinetic energy carried by the granular particles to the elastic guides through their lateral interactions. If we apply a small-amplitude impact to a curved granular chain, the amount of energy absorbed by the elastic guides is relatively small due to the weak perturbations experienced by the elastic guides. However, if a large-amplitude impact is applied to the curved granular

chain, the elastic guides deform significantly during the short impact event, and a large portion of the kinetic energy is dispensed to the elastic guides due to the structural deformation of the elastic guides. This means that the elastic guides present an improved efficiency of energy absorption under large dynamic disturbances relative to that of small excitations. In [26], such amplitude-dependent behavior in a monodispersed granular chain has been experimentally and numerically verified using high-speed photography, and the feasibility of tuning the efficiency of the energy absorption was demonstrated by manipulating the initial curvature of the granular system.

The frequency spectra of transmitted waves under various impactors are shown in Fig. 11 as a function of striker masses and frequency components. Both numerical and experimental results are based on the FFT of time-domain signals, which are normalized with respect to their maximum PSD values. For the straight chain, we observe the presence of the optical and acoustic pass-bands in the low range of striker masses (see Fig. 11(a)). Here the yellow dotted lines represent the cutoff frequencies predicted analytically. As the striker mass increases, however, the distinction between pass- and stop-bands becomes less evident. This is consistent with the results observed in the previous section that discussed the effect of system nonlinearity on frequency band structures by altering pre-compression. We also find that most energy is concentrated in the near-zero frequency domain when the system is excited by large-amplitude impacts, while the transmitted energy is distributed in the pass-bands when the system is excited by small-amplitude impacts. This means that the transmitted waves exhibit distinctive energy distribution in the frequency domain, which is highly dependent on the impact amplitude simulated by various striker masses. Figure 11(b) shows the frequency responses of the curved chain ($\Delta=58.9$ mm) under various impacts. We again confirm the presence of frequency band structures resulted from the dispersive effect of propagating waves under the light-striker impacts. In comparison to the straight chain, the band structure is down-shifted, which is in agreement with the findings in the previous section. We perform numerical simulations using the combined DE and FE model, and the results are shown in Figs. 11(c) and (d). We find that the numerical results corroborate the experimental results satisfactorily both in the straight and curved chains.

The experimental and numerical results in this section confirm the amplitude- and frequency-dependent behavior of a curved granular chain. We observe an evident frequency band structure in the linear regime, which can be tuned by manipulating the initial curvature of the bent chains. We also witness the formation of highly nonlinear solitary waves in the nonlinear regime, whose transmission efficiency is critically determined by the amplitude of external impacts. This study establishes a foundation for utilizing the combined

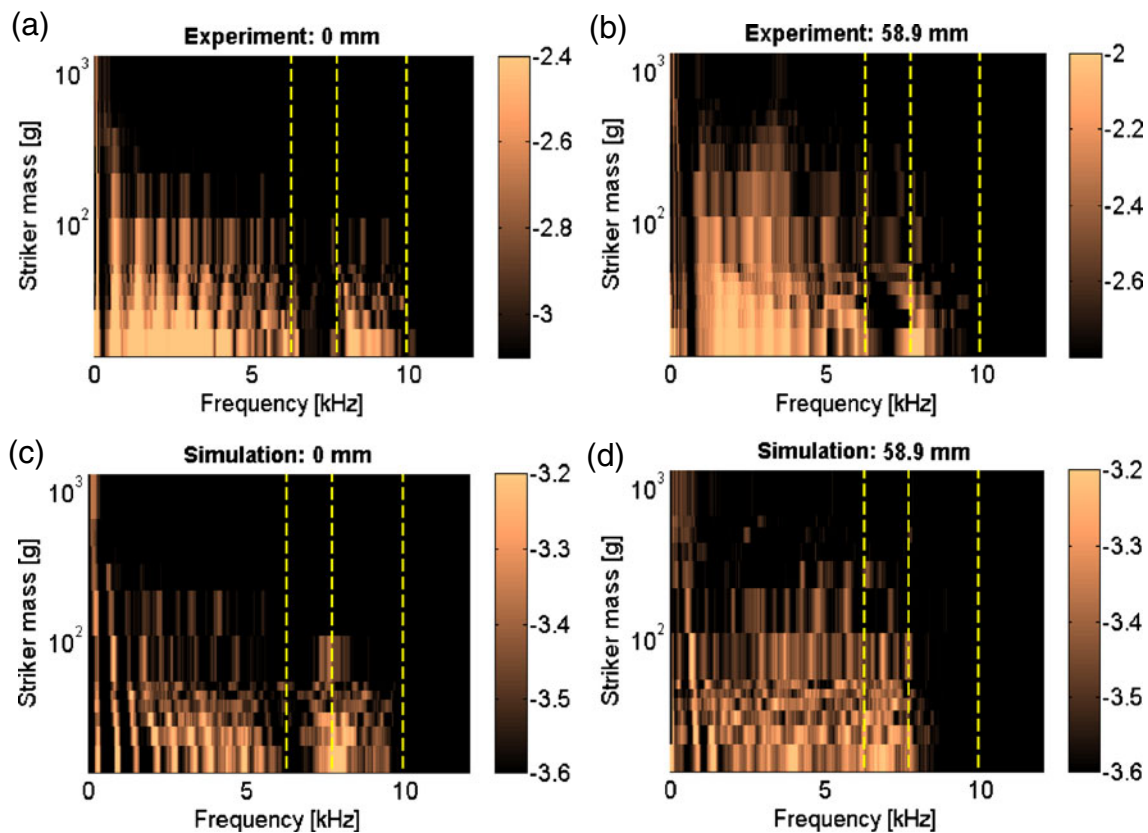


Fig. 11 Experimental (*top row*) and numerical (*bottom row*) surface plots of PSD for straight (*left column*) and curved (*right column*) chains. Each surface plot depicts the force profiles of all 13 striker impacts after being normalized with respect to their maximum PSD values. The dashed yellow lines denote the band edges of acoustic and optical pass bands predicted by analysis

granular and elastic system as a novel structural material for engineering applications.

Conclusions

In this work, we demonstrated the frequency- and amplitude-dependent filtering properties of compressive stress waves transmitted through one-dimensional curved granular crystals composed of diatomic particles. The granular crystals studied consist of periodic arrays of alternating spherical and cylindrical particles, which are constrained by bent elastic guides. When external excitations are applied to the chains, the elastic guides can flex and absorb impact energy by converting the particles' kinetic energy to potential energy via structural deformation. Under small-amplitude disturbances relative to the static pre-compression, the combined granular and linear elastic system can transmit and support linear elastic waves, leading to the formation of acoustic band structures with allowable and forbidden frequency bands. These band structures can be tuned by manipulating the amount of the static pre-compression or the chain

curvature initially imposed to the diatomic granular system. Hence, the combined granular and linear elastic media are capable of filtering a selected range of frequencies contained in external impacts. Upon the excitation by large-amplitude impacts, this hybrid system can generate and propagate compactly-supported nonlinear waves in the form of solitary waves. In this case, the amount of energy transmitted through the granular system is critically dependent on the wave amplitude, and the combined granular and linear elastic structure performs as an amplitude-dependent filter. We show that the efficiency of the energy transmission can be tuned via simple manipulation of the curvature of the granular system.

The findings of this work suggest the use of hybrid granular and soft elastic media in engineering applications, such as tunable protective devices and impact mitigating structures that can selectively allow or reject the transmission of external impacts. The characteristics of these new structures can be tailored by varying material types, geometry, and boundary conditions. In particular, by including materials of contrasting properties (e.g., soft vs. rigid elements), these structures can present unique combinations of mechanical properties unprecedented in other mechanical

systems. This study is limited to the construction of a one-dimensional granular crystal, but the mechanism developed in this study can be extended to a three-dimensional architecture, for example by arraying the granular crystals in elastic matrices. This can lead to the development of tunable and lightweight materials system that can form innovative structures used in space, civil infrastructure, and biomedical applications.

Acknowledgements We acknowledge support from DARPA (Contract N. HR0011-10-C-0089, Dr. Jinendra Ranka), the National Science Foundation, Grant Number CMMI-0844540 (Career), and the Army Research Office (MURI grant US ARO W911NF-09-1-0436, Dr. David Stepp).

References

- Nesterenko VF (1983) Propagation of nonlinear compression pulses in granular media. *J Appl Mech Tech Phys* 24:733–743
- Nesterenko VF (2001) *Dynamics of Heterogeneous Materials*. Springer-Verlag New York, Inc, New York
- Coste C, Falcon E, Fauve S (1997) Solitary waves in a chain of beads under Hertz contact. *Physical Review E* 56(5):6104–6117
- Chatterjee A (1999) Asymptotic solution for solitary waves in a chain of elastic spheres. *Physical Review E* 59(5):5912–5919
- Sen S, Hong J, Bang J, Avalos E, Doney R (2008) Solitary waves in the granular chain. *Physics Reports* 462(2):21–66
- Daraio C, Nesterenko VF, Herbold EB, Jin S (2005) Strongly nonlinear waves in a chain of Teflon beads. *Physical Review E* 72(1):016603
- Jaeger HM, Nagel SR, Behringer RP (1996) Granular solids, liquids, and gases. *Rev Mod Phys* 68(4):1259–1273
- Sokolow A, Bittle EG, Sen S (2007) Solitary wave train formation in Hertzian chains. *EPL (Europhysics Letters)* 77(2):24002
- Manciu M, Sen S, Hurd AJ (2001) Crossing of identical solitary waves in a chain of elastic beads. *Physical Review E* 63(1):016614
- Herbold EB, Nesterenko VF (2007) Shock wave structure in a strongly nonlinear lattice with viscous dissipation. *Physical Review E* 75(2):021304
- Molinari A, Daraio C (2009) Stationary shocks in periodic highly nonlinear granular chains. *Physical Review E* 80:056602
- Avalos E, Sen S (2009) How solitary waves collide in discrete granular alignments. *Physical Review E* 79(4):046607
- Santibanez F, Munoz R, Caussariou A, Job S, Melo F (2011) Experimental evidence of solitary wave interaction in Hertzian chains. *Physical Review E* 84(2):026604
- Sen S, Mohan TRK, Donald P, Visco J, Swaminathan S, Sokolow A, Avalos E, Nakagawa M (2005) Using Mechanical Energy as a Probe for the Detection and Imaging of shallow Buried Inclusions in Dry Granular Beds. *Int J Mod Phys B (Singapore)* 19(18):2951–2973
- Spadoni A, Daraio C (2010) Generation and control of sound bullets with a nonlinear acoustic lens. *Proc Natl Acad Sci U S A* (107), pp. 7230–7234.
- Sen S, Manciu FS, Manciu M (2001) Thermalizing an impulse. *Physica A: Statistical Mechanics and its Applications* 299(3–4):551–558
- Hong J (2005) Universal power-law decay of the impulse energy in granular protectors. *Physical Review Letters*, 94,108001(10)
- Daraio C, Nesterenko VF, Herbold EB, Jin S (2006) Energy trapping and shock disintegration in a composite granular medium. *Phys Rev Lett* 96(5):058002
- Melo F, Job S, Santibanez F, Tapia F (2006) Experimental evidence of shock mitigation in a Hertzian tapered chain. *Physical Review E* 73(4):041305
- Fraternali F, Porter MA, Daraio C (2009) Optimal Design of Composite Granular Protectors. *Mech Adv Mater Struct* 17(1):1–19
- Khatri D, Rizzo P, Daraio C (2008) Highly nonlinear waves' sensor technology for highway infrastructures. *SPIE Smart Structures/NDE*, 15th annual international symposium San Diego, CA, 6934-6925
- Yang J, Silvestro C, Sangiorgio S, Borkowski S, Ebramzadeh E, De Nardo L, Daraio C (2012) Nondestructive evaluation of orthopedic implant stability in THA using highly nonlinear solitary waves. *Smart Materials and Structures* 21:012001
- Yang J, Sangiorgio S, Silvestro C, De Nardo L, Daraio C, Ebramzadeh E (2012) Site-specific quantification of bone quality using highly nonlinear solitary waves, *Journal of Biomechanical Engineering* (in print).
- Herbold E, Kim J, Nesterenko V, Wang S, Daraio C (2009) Pulse propagation in a linear and nonlinear diatomic periodic chain: effects of acoustic frequency band-gap. *Acta Mechanica* 205(1):85–103
- Boechler N, Yang J, Theocharis G, Kevrekidis PG, Daraio C (2011) Tunable vibrational band gaps in one-dimensional diatomic granular crystals with three-particle unit cells. *J Appl Phys* 109(7):074906–074907
- Yang J, Dunatunga S, Daraio C (2012) Amplitude-dependent attenuation of compressive waves in curved granular crystals constrained by elastic guides. *Acta Mechanica* 223(3):549–562
- Yang J, Silvestro C, Khatri D, De Nardo L, Daraio C (2011) Interaction of highly nonlinear solitary waves with linear elastic media. *Physical Review E* 83:046606
- Johnson KL (1985) *Contact mechanics*. Cambridge University Press.
- Porter MADC, Szelengowicz I, Herbold EB, Kevrekidis PG (2009) Highly Nonlinear Solitary Waves in Heterogeneous Periodic Granular Media. *Physica D* 238:666–676
- Porter MA, Daraio C, Herbold EB, Szelengowicz I, Kevrekidis PG (2008) Highly nonlinear solitary waves in periodic dimer granular chains. *Physical Review E* 77:015601
- Jayaprakash KR, Starosvetsky Y, Vakakis AF (2011) New family of solitary waves in granular dimer chains with no precompression. *Physical Review E* 83(3):036606
- Brillouin L (1953) *Wave Propagation in Periodic Structures*. Dover, New York
- Phani AS, Fleck NA (2008) Elastic boundary layers in two-dimensional isotropic lattices. *J Appl Mech* 75(2):021020–021028
- Cundall PA, Strack ODL (1979) A discrete numerical model for granular assemblies. *Geotechnique* 29(1):47–65
- Tsuji Y, Tanaka T, Ishida T (1992) Lagrangian numerical simulation of plug flow of cohesionless particles in a horizontal pipe. *Powder Technol* 71(3):239–250
- Gere JM, Timoshenko SP (1997) *Mechanics of materials*, Pws Pub Co.
- Carretero-González R, Khatri D, Porter MA, Kevrekidis PG, Daraio C (2009) Dissipative solitary waves in granular crystals. *Phys Rev Lett* 102(2):024102
- Lamb GL (1980) *Elements of soliton theory*, John Wiley & Sons Inc.
- Scott A (2003) *Nonlinear science: emergence and dynamics of coherent structures*, Oxford University Press.
- Dauxois T, Peyrard M (2006) *Physics of solitons*, Cambridge University Press
- Daraio C, Nesterenko VF, Herbold EB, Jin S (2006) Tunability of solitary wave properties in one-dimensional strongly nonlinear phononic crystals. *Phys Rev E* 73(2):026610
- Job S, Melo F, Sokolow A, Sen S (2007) Solitary wave trains in granular chains: experiments, theory and simulations. *Granul Matter* 10:13–20